ACS Sustainable Resource Management

pubs.acs.org/acssrm

Article

Microalgae for the Extraction and Separation of Rare Earths: An STXM Study of Ce, Gd, and P

Maxence Plouviez, Benoit Guieysse, Karla Wolmarans, Andrea Marie E. Matinong, Olivia Buwalda, Karina Thånell, Igor Beinik, J. R. Marius Tuyishime, Valerie Mitchell, Peter Kappen, David Flynn, Thierry Jauffrais, and Richard G. Haverkamp*

Cite This: https://doi.org/10.1021/acssusresmgt.4c00237

Read Online

ACCESS | Metrics & More | Article Recommendations

ABSTRACT: Rare earth elements (lanthanides) are critical materials for many applications, particularly those involved in new energy. Extracting these elements economically from low-concentration sources may be challenging. This study investigates the interaction of Ce and Gd with microalgae that have been triggered to form phosphate-rich granules. Lanthanides usually occur in nature as phosphates, and therefore, we hypothesized that phosphate accumulation in microalgae may facilitate lanthanide sequestration. Synchrotron-based scanning transmission X-ray microspectroscopy (STXM) was used to map the distribution of Gd, Ce, and P in and around cells of *Chlamydomonas reinhardtii*. STXM provided X-ray absorption (XAS) spectra at the Gd $M_{4,5}$-edge, the Ce $M_{4,5}$-edge, and the P K-edge, supported by bulk X-ray absorption spectroscopy at another beamline, and elemental maps from scanning electron microscopy with energy-dispersive spectroscopy (SEM/EDS). Gd was associated with P in polyphosphate granules within *C. reinhardtii* and with P outside the cells. Ce was associated with P outside the microalgal cells but not with the P granules inside the cells. Gd and Ce were found to react with phosphate to form a distinct compound apparent in X-ray absorption near edge spectroscopy (XANES) of bulk samples. However, this compound is not found in the P granules that are coincident with Gd inside the alga. These differences in uptake by the microalga between Ce and Gd may suggest a selective extraction technique and could be generalized to other rare earth elements that are otherwise hard to separate.

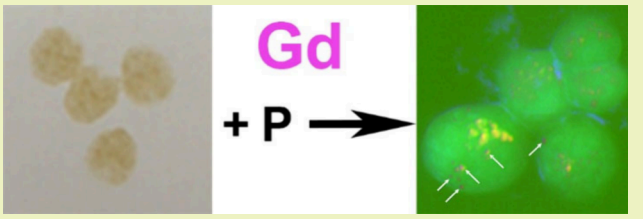

KEYWORDS: *Lanthanide, cerium, gadolinium, phosphorus, XAS, XAFS, Gd M5-edge, Ce M5-edge, P K-edge*

INTRODUCTION

Demand for lanthanides (rare earth elements) has increased, driven by technological applications including energy applications, electronic devices, and lighting and displays (i.e. batteries, magnets, and phosphors), and their continued use as catalysts.[1] There is a limited range of concentrated ore deposits worldwide.[2] Geopolitical considerations[3] are driving the need to find new deposits, which might include lower-concentration sources, including byproduct streams from other extraction processes.[4] These lower-concentration streams require new extraction methods for lanthanides, including greener and more sustainable methods,[5] as well as urban mining[6] and biomining.[4]

Lanthanides can be adsorbed or absorbed by algae.[7] If the adsorption or absorption are significantly different for different lanthanides, these mechanisms may provide a possible way to selectively extract and concentrate lanthanides. For example, red algae have been investigated for removal of Y, Ce, Eu, and Tb from solution,[8] and from wastewater for La, Y, and Sm,[9] and La, Y, Ce, Nd, and Eu.[10] Dead cyanobacteria have also been used for the removal of Ce by adsorption from wastewater.[11]

The storage sites for lanthanides within plants have been investigated in some studies. For example, La, Gd, Nd, and Ce were found to accumulate in the green alga *Desmodesmus quadricauda*, with La and Gd stored in the cytoplasm and Nd and Ce concentrated in the chloroplasts.[12] Similarly, in the green alga *Euglena gracilis*, Nd concentrates in the chloroplasts.[13] With the red alga *Galdieria sulphuraria*, it has been proposed that La, Y, and Sm are either physically adsorbed onto the alga surface or absorbed by exchange with Ca^{2+}, although this is confounded by the presence of Ca-alginate beads as supports for the alga.[9]

Lanthanides are most commonly found in nature with phosphates (in the minerals monazite and xenotine). Lanthanide phosphate can be precipitated from aqueous

Received: June 14, 2024
Revised: October 7, 2024
Accepted: October 8, 2024

solution for all the lanthanides,[14] with the affinity for phosphate increasing along the lanthanide series from La to Lu for the Ln^{3+} ions with phosphate receptor ligands.[15] Therefore, it is reasonable to suppose that the presence of phosphate may enhance the uptake of lanthanides by algae. Unicellular algae can be stimulated to form polyphosphate granules, including *Chlamydomonas reinhardtii*, *Desmodesmus armatus*, *Gonium pectorale*, and *Microcystis aeruginosa*.[16,17]

Scanning transmission X-ray microspectroscopy (STXM) can map the distribution of elements, including P, Gd, and Ce, at a sub-μm scale.[18] STXM generates a map of X-ray absorption spectra (XAS) for one element per energy range selected. These XAS spectra can be interpreted to selectively plot the distribution of chemical species of an element of interest. STXM can therefore map elemental distribution, or chemical distribution, within the constraints of XAS.[19] SEM/EDS can also be used to map concentrations of the elements (although in our system at lower spatial resolution and with lower sensitivity than STXM), however, EDS does not provide chemical information.

We hypothesized that high levels of P in algae, as can be achieved through the formation of polyphosphate granules, could assist in the intracellular accumulation of lanthanides. In our study, we stimulated a microalga to produce P-rich granules and we inoculated that microalga with Gd or Ce. We then measured the fate of Gd or Ce, in particular whether they were associated with the phosphate granules found in the unicellular green algae *C. reinhardtii*.

Chlamydomonas reinhardtii was selected because it is a model organism capable of synthesizing polyphosphate when transitioning from P deplete and P replete conditions.[20] A light lanthanide, Ce, and a heavier lanthanide, Gd, were selected to compare the compartmentalization of lanthanides in an alga using STXM, XAS, and scanning electron microscopy with energy-dispersive spectroscopy (SEM/EDS).

MATERIALS AND METHODS

Cultures. *Chlamydomonas reinhardtii* (CC-1690) culture maintenance and cultivation were performed as described previously.[20] Briefly, the microalga was sequentially cultivated on low-phosphorus (1 mg P·L^{-1}) minimal media (triplicates with final volume of 600 mL). The day of the experiment, 25 mL of culture was used to analyze the initial dry weight, optical density, total phosphorus, and dissolved phosphate, and for microscopic observations.[20] Algal cultures were then supplemented with a P dose equivalent to a final concentration of 10 mg P·L^{-1}, using a 1 M stock solution of potassium phosphate (46 g·L^{-1} KH_2PO_4 and 115 g·L^{-1} K_2HPO_4) and either $GdCl_3$ or $CeCl_3$ at a final concentration of 10 mg·L^{-1} and 6 mg·L^{-1} (38 μM and 24 μM respectively). After incubation for 5 h, 25 mL of culture was used for the same analysis as above. The P content in the biomass (g-P·g-dry weight $^{-1}$, expressed as%) was calculated as the difference between the total P concentration in the culture (g P·L^{-1}) and the dissolved phosphate concentration in solution (g P·L^{-1}) divided by the cell dry weight concentration (g-dry cells·L^{-1}).

At the end of the incubation period, the remaining cultures were harvested by centrifugation at 10,000 g for 3.5 min (Sigma 6-16 centrifuge) in several batches. The pellets were rinsed with distilled water and centrifuged again, before being mixed to make a composite sample and frozen at -80 °C. The algae pellets were finally freeze-dried in a Buchi Lyovapor L-300 for 36 h at 0.2 mbar, with a temperature profile starting at -30 °C and finishing at 20 °C.

STXM. STXM images were recorded at the SoftiMAX beamline of MAX IV synchrotron, Lund, Sweden,[18] which has an elliptically polarizing undulator (APPLE-II type) with a 48 mm period. Here, the third harmonic was used for the P K-edge energy range, and for the Gd and Ce $M_{4,5}$-edge energy ranges, with Rh-coated mirrors. A 50 nm outer-zone width, high-energy Fresnel zone plate (Au) was used as the final focal element (B. Rösner, PSI, Switzerland). Signal acquisition was by photomultiplier tube detector consisting of a Hamamatsu H3164-10 with a P43 scintillator. The beamline provides an energy resolution of $\geq$5000 $E/\Delta E$ at energies above 2 keV. The flux at the sample was better around 1×10^9 ph/s. Images were recorded with a step size of 30−100 nm.

Each STXM dataset consists of a stack of images, each taken at a specific X-ray energy so that XAS spectra are collected for each point in the image. Energy steps between the images in a stack varied to provide a pre-edge wide-spaced region, a tight energy spacing over the edge, and a wider energy spacing after the edge. Typically, 160 energy points were recorded for a STXM stack. The three-dimensional dataset is versatile: either individual images can be displayed, or for example, an image extracted from a combination of images taken at different energies can be displayed. XAS spectra can be obtained from this data, either for a point in space on the image stack or a region in space on the image stack. Because of small sample/beam drift between images, image stack alignment was performed prior to extracting XAS spectra or mapping spectral regions. Spectra were normalized through dividing by a measurement over empty regions using the same energy/dwell-time parameters.

The P K-edge energy was calibrated against tetraphenylphosphonium bromide (PPh_4Br) (SigmaAldrich).[21] This work was the first use of P K-edge STXM at this beamline and formed part of the commissioning.

Samples were mounted on 200 nm-thick windows of Si_3N_4 (Silson, UK) by dispersing in water, dropping onto the window, and leaving to air-dry. Standards for XAS spectra were also recorded (with minimal image sizes) with the compounds adenosine 5′-triphosphate disodium salt hydrate (SigmaAldrich), sodium phosphate glass (SigmaAldrich), phytic acid sodium salt (SigmaAldrich), and azolectin from soybean.

Matched images of P and Ce and of P and Gd were taken on the same sample regions. Three energy ranges were used. For the Gd M_5-edge, an energy range of approximately 1175−1236 eV was used; for the Ce $M_{4,5}$-edge, an energy range of approximately 872−923.5 eV was used, and for the P K-edge, an energy range of 2148−2200 eV was used. In the case of the P K-edge, this was not optimized and gave barely enough pre-edge for normalization. The P K-edge energy was calibrated against PPh_4Br.[21] However, this was done as part of a larger suite of diverse samples with large energy range changes, and calibration was not performed immediately preceding the measurements, with the estimated precision of calibration being ±1 eV for the P K-edge. No calibration was run for the Gd M_5-edge or Ce M_5-edge; these were adjusted in the displayed plots for the edges to be +1.5 eV compared with accepted values for the elements, as an approximation, supposing that these might be present as phosphates.

Data processing of the STXM used aXis2000 software.[22] This involved removing "bad lines" or "bad points" from individual images, aligning the image stack, selecting background and regions of interest for XAS spectra extraction from the image stack, and plotting chemical maps from spectrum fits. Athena[23] software was subsequently used for further XAS spectra processing taken from the STXM data with the aXis2000 software.

XAS/XANES. XAS (specifically XANES or NEXAFS) at the P K-edge was recorded on the MEX2 beamline at the Australian Synchrotron. This beamline uses medium- to low-energy monochromatic X-rays from an Si(111) double crystal monochromator ($dE/E \approx 1.4 \times 10^{-4}$) at a fixed offset and with a beam size of 3×5 mm^2 and photon flux around 5×10^{10} ph^{-1} s^{-1}. Spectra were recorded at room temperature in a vacuum ($\leq 1 \times 10^{-5}$ Pa). Samples of microalgae or standard compounds were mounted on conductive carbon tape on a stainless-steel ruler and analyzed in fluorescence mode. The P K-edge energy was calibrated against the first pre-edge feature of PPh_4Br (2146.96 eV).[21] This was a commissioning experiment for P K-edge energy at the beamline.

XAS at the Gd M_5-edge and Ce M_5-edge were recorded on the MEX1 beamline at the Australian Synchrotron. Standard compounds were diluted with cellulose, samples were not diluted, and both were pressed into pellets for analysis, and were measured in transmission

https://doi.org/10.1021/acssusresmgt.4c00237
ACS Sustainable Resour. Manage. XXXX, XXX, XXX−XXX

mode. The beamline produces X-rays from a bending magnet, with an Si(111) double crystal monochromator providing an energy resolution ($\Delta E/E$) of 1.4×10^{-4}. The beam size on the sample was 0.5×3 mm, with a photon flux 3×10^{10} ph^{-1} s^{-1}. Co or Cr metal foil placed before the last ion chamber was used as an energy reference with each sample for Gd and Ce, respectively. Samples that were low in Gd and Ce were also run in fluorescent mode using a four-element silicon solid-state detector.

Athena[23] software was used to process XAS spectra collected on both the XAS beamline and extracted from the STXM stacks, and to compare spectra from both sources. Athena was used for background removal, with E_0 unconstrained, and for spectra normalization and comparisons.

SEM/EDS. SEM images and EDS maps were recorded using a JSM 6500F SEM (JEOL Engineering Co. Ltd, Japan) equipped with a JEOL Dry SD Extra EDS Detector for elemental analysis operated at 15 kV. Samples of algae were mounted on aluminum stubs on conductive adhesive tape. An elemental distribution map was recorded for the Gd-containing *C. reinhardtii* sample but not for the Ce-containing sample. Data were processed using the JED Series Mapping Program (JEOL Engineering Co. Ltd, Japan) that is supplied with the instrument.

Inductively Coupled Plasma Mass Spectrometry (ICP-MS). The samples were prepared using the following method. The sample (1.0 mg) was added to a 15 mL centrifuge tube and 1.5 mL 69% HNO_3 Tracepur (Merck, Germany) and 0.5 mL 37% HCl Tracepur (Merck, Germany) were added. The vessels were sealed and placed in 100 °C water bath for 30 min. The digest was diluted with 13 mL Type-1 water to 15 mL final volume. The solutions were quantitatively analyzed for desired elements on an Agilent 7700 ICP-MS in He mode to reduce polyatomic interferences. Calibration standards were prepared in a matrix-matched solution from 1000 ppm single-element standards (CPI International, USA). A 20 ppb solution of yttrium was used to monitor drift and matrix effects. All results are in μg/g and have been back-calculated to the original sample.

RESULTS

P, Gd, and Ce Accumulation in *Chlamydomonas reinhardtii* Samples. The transition from P deplete to P replete conditions in the absence of added rare earths triggered P accumulation in *C. reinhardtii* up to 2.50 ± 0.42%P (as g-P·g^{-1}). Similar concentrations were measured for the cultures supplemented with P and the rare earths (2.60 ± 0.01%P and 2.40 ± 0.31%P for the samples supplemented with Gd and Ce, respectively). ICP-MS analysis of dried *C. reinhardtii* samples showed that the microalga supplemented by both P and either Ce or Gd accumulated Ce (0.57 ± 0.54%Ce as g-Ce·g^{-1}) and Gd (1.5 ± 0.9%Gd as g-Gd·g^{-1}). This absorption amounts to 17% of the Ce and 27% of the Gd available from solution. The addition of Gd and Ce did not diminish the optical density of the algal suspensions, indicating that the level of these elements was not toxic to the cells (Table 1).

STXM. Images of *C. reinhardtii* were obtained from STXM at each of the elemental X-ray absorption edges investigated, with well-matched images of the same physical region recorded at the different energy ranges (Figure 1a for the P K-edge, Figure 1b for the Gd $M_{4,5}$-edge).

Table 1. Initial and Final Optical Densities (at 683 nm) of *Chlamydomonas reinhardtii* Cultures Supplied 10 mg-P·L^{-1} and Either Gadolinium (10 mg·L^{-1}) or Cerium (6 mg·L^{-1})[a]

	0 h	5 h
Control (+P)	0.43 ± 0.01	0.47 ± 0.02
Gd (+P)	0.44 ± 0.01	0.48 ± 0.01
Ce (+P)	0.44 ± 0.01	0.48 ± 0.01

[a]Data represent the average and standard deviation from 6 measurements.

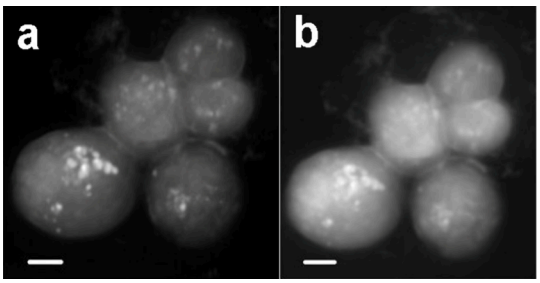

Figure 1. Gadolinium with *Chlamydomonas reinhardtii* 1690, STXM optical density image of total X-ray absorption over: (a) the P combined K-edge region; and (b) the Gd combined $M_{4,5}$-edge region. Scale bar 2 μm.

By selecting an energy window around the main white line for each of the elements (Gd and P for one sample, and Ce and P for the other sample), the locations of these elements in the sample becomes apparent.

For *C. reinhardtii* treated with Gd, polyphosphate granules were visible in the cells. These showed up distinctly in the STXM P K-edge maps and had a range of diameters up to 1 μm (Figure 2a). Phosphorous was not visible outside the cells.

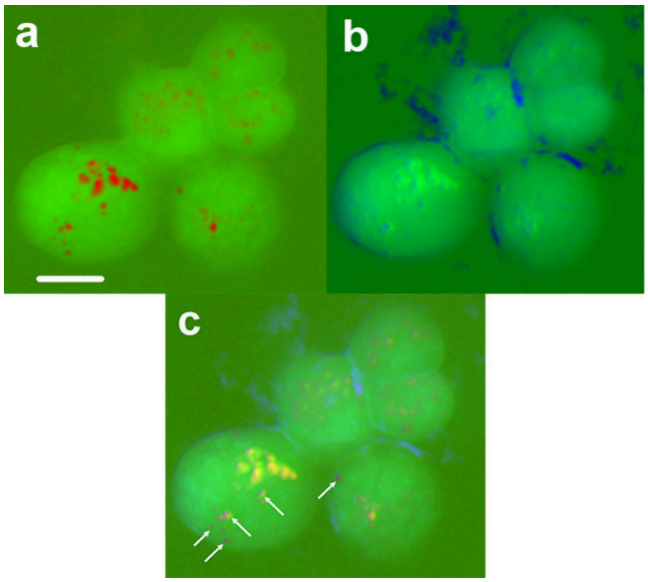

Figure 2. Distribution of phosphorus and gadolinium in *Chlamydomonas reinhardtii* 1690. STXM maps: (a) the P K-edge region (red); (b) the Gd M_5-edge region (blue); (c) composite image of P and Gd, where purple represents regions where both Gd and P are present (some of these are indicated with arrows). Scale bar 4 μm.

The Gd also shows up clearly in the STXM maps (Figure 2b), with most of the Gd observed outside the cells, being either closely associated with the cell walls (perhaps adsorbed) or free from the cells on the sampling SiN mounting window. The process of dispersing the algae in water, then drying them on the SiN window, may have caused some of the surface material of the cells to dislodge and become attached to the sampling mounting window. Of more significance is the co-location of some Gd with P granules; this is observed in the composite

https://doi.org/10.1021/acssusresmgt.4c00237
ACS Sustainable Resour. Manage. XXXX, XXX, XXX−XXX

image with both P and Gd, where the combination gives a purple hue (Figure 2c).

For *C. reinhardtii* treated with Ce, polyphosphate granules were visible in the cells. These showed up distinctly in the STXM P K-edge maps and had a range of diameters up to 0.6 μm (Figure 3a). In contrast to the cells treated with Gd, phosphorus was visible outside the cells, with some of this being closely associated with the outer cell walls (Figure 3b). In contrast to the cells treated with Gd, Ce was not found in the cells and was not associated with the P granules. Ce is found outside the cells and was closely associated with extracellular P. Therefore, there appear to be Ce phosphate deposits outside the cells, some of which appear to have become dislodged onto the sampling SiN mounting window.

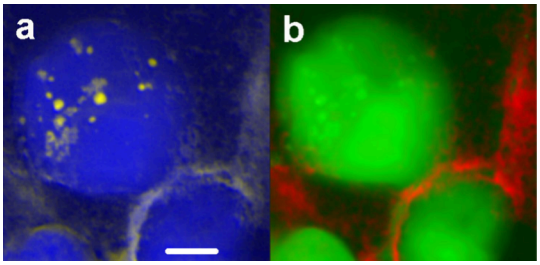

Figure 3. Distribution of phosphorus and cerium in *Chlamydomonas reinhardtii* 1690. STXM maps for: (a) the P K-edge region (yellow); (b) the Ce M_5-edge region (red). Scale bar 2 μm.

XAS from STXM. The XAS spectra extracted from the STXM data are presented in Figure 4. The Ce energy scan covers both the M_4-edge and the M_5-edge (Figure 4a). The spectrum, which is very similar to that published for $CeCl_6^{3-}$,[24] where Ce is in the Ce^{III} formal oxidation state, provides evidence that the Ce in the microalgal samples is in the expected Ce^{3+} state. The XAS represents "a transition from single $3d^{10}4f^1$ initial state to the multiplet states associated with a $3d^9 4f^2$ final state configuration".[24] The Ce chemistry does not appear to vary between sites in the samples, with similar XAS spectra close to the cells or on a separate region. We expect that the Ce is in the form of a chloride or phosphate in the samples presented here, although this warrants a deeper investigation.

The Gd energy scan covering both the M_4-edge and the M_5-edge was collected with a limited number of energy steps to reduce the collection time (Figure 4b). The Gd M_5-edge consists of the promotion of a $3d^{10}4f^7$ initial state to a $3d^9 4f^8$ final state configuration. The energy features in the Gd XANES region are similar in the P granules, the Gd-rich region between the cells, and the area away from the cells, meaning that the P−Gd complex found in the different areas has a similar chemical structure. A detailed study of the XAS of $Gd_3Ga_5O_{12}$ provides a superficially similar XANES spectrum to that observed here,[25] although we expect that the Gd is in the form of a salt of either chloride or phosphate in the algae samples. As for Ce, this warrants a deeper investigation. A low-resolution Gd M_5-edge XAS spectrum for GdTiGe[26] also appears superficially similar, while an XAS of Gd $M_{4,5}$ for $Ce_{1-x}Gd_xO_2$[27] has a lower resolution. Consequently, it is difficult to make a comparison between the chemistry of those compounds and the samples measured here from those spectra. The published data on Gd M_5-edge XANES suggest that there are not large changes in the XAS spectrum with changes in chemistry, and therefore that it is not a sensitive indicator for subtle chemistry changes, although it should be noted that these data are very limited.

The P K-edge spectra for the P in the Gd- and Ce-supplemented microalgae samples were recorded with barely sufficient pre-edge region (Figure 4c,d). Other more detailed

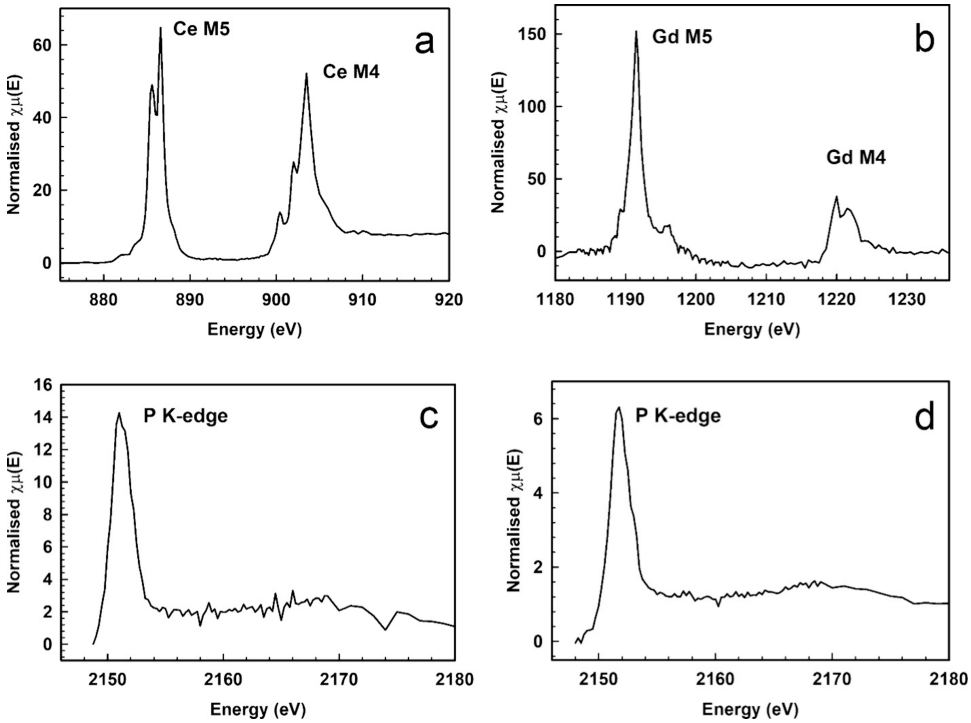

Figure 4. XAS from STXM of algae. (a) Ce $M_{5,4}$-edge normalized to M_5. (b) Gd M_5-edge, granule. (c) P K-edge for Gd-containing algae, granule. (d) P K-edge for Ce-containing algae, granule.

https://doi.org/10.1021/acssusresmgt.4c00237
ACS Sustainable Resour. Manage. XXXX, XXX, XXX−XXX

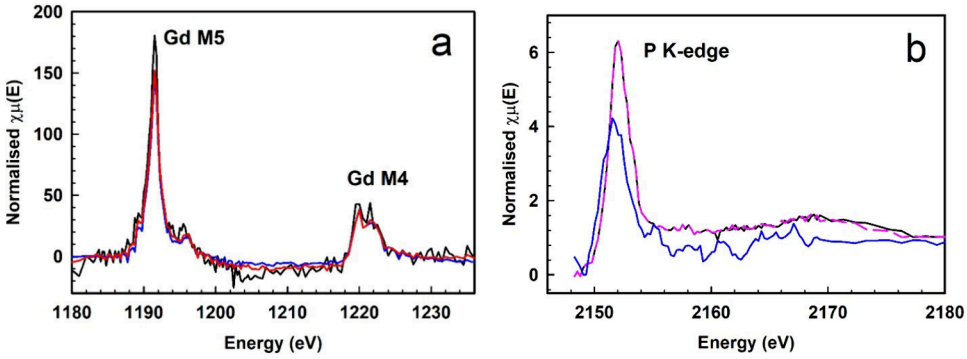

Figure 5. (a) Gd $M_{5,4}$-edge comparison. P granule—black line, deposit between cells—blue line, deposit outside and away from cells—red line. (b) P K-edge for P granule with co-located Gd and P — black line; P granule in Ce sample—dashed pink line; P-containing area between cells with co-located Ce and P — blue line (a five-point average).

work on similar samples with STXM and dedicated XAS bulk analysis has shown the P-containing granules to be a phosphate compound, likely a polyphosphate of a complex nature similar to phytic acid,[17] and the spectra extracted here from STXM are consistent with this prior work. The P K-edge XAS of the P-containing granules is similar in both the Gd- and Ce-containing algae.

We again caution that the energy for the Ce and Gd M-edges presented here were not subjected to precise energy calibration.

To observe chemical changes with the association of P with Gd or Ce, a comparison was made between XANES spectra extracted from STXM for different regions, including the P granules and regions outside the P granules (Figure 5). For the Gd $M_{4,5}$-edge, no observable differences were recorded when comparing a P granule with co-located Gd and Gd outside the cells where P is not obviously present (Figure 5a). However, it is important to note that the lanthanide M-edge is not a very sensitive indicator for phosphate compounds.[28]

For the P K-edge, a P granule with co-located Gd, a P granule in the Ce sample with no co-located Ce, and a region containing P and Ce outside the cells (between two microalgal cells) were compared (Figure 5b). P granules, both with and without co-located rare earth, give the same XANES spectrum, while the P and Ce region outside the cells provided a P spectrum (after a five-point averaging) that is too noisy to draw any inferences.

XAS (Bulk, P K-Edge). STXM was unable to distinguish differences in the chemistry of cell areas when lanthanides and phosphate are co-located. Therefore, a spatially unresolved, but more chemically sensitive, technique of bulk P K-edge XANES was performed on algae samples on a dedicated XAS beamline (MEX2). *C. reinhardtii* samples with or without Gd or Ce were analyzed. These are plotted in Figure 6, along with a XANES spectrum extracted from STXM for *C. reinhardtii* with no rare earths added. The STXM-derived XANES and the XAS beamline XANES match very well for the microalga without rare earths. There are, however, clear differences between P in XANES when either Gd or Ce is present, with a different shape (a less steep transition from the white line to higher energy) and an extra peak at 2162 eV. These are a strong indication that a different P-compound is present in microalgae containing Gd or Ce than in those without these elements. When Gd and Ce are not present, the P is likely in the form of inorganic polyphosphates or organic polyphosphate such as phytic acid.[17] An obvious candidate when either Gd or Ce are present might be a Gd or Ce phytate or simple phosphate complex, but we did not have any material available as reference standards to confirm this and were not able to find XANES of these compounds in the literature. In addition, while Gd and Ce react with phosphate to form a distinct compound apparent in XANES of bulk samples, this compound is not found in the P granules that coincide with Gd inside the algae.

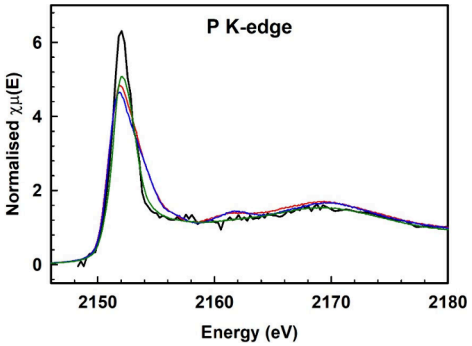

Figure 6. P K-edge XANES of bulk samples for *Chlamydomonas reinhardtii*, with no added rare earth element (green line), with Ce added (red line) and with Gd added (blue line), compared with the XANES taken from microscopic STXM at just the location of a P granule (black line).

SEM/EDS. EDS maps recorded for *C. reinhardtii* treated with Gd support the STXM maps, with P granules present (Figure 7) and likely *inside* the cell, but this cannot be confirmed from the EDS images. However, the sensitivity to Gd is not high, and an association of Gd with the P granules is not visible. These maps do show a region where Gd and P are closely associated, and this appears to be outside the algal cells on the sample holder. It is noteworthy that we did not observe this with these samples in STXM, although it was possible to record only a limited number of STXM images.

DISCUSSION

The microalga *C. reinhardtii* has previously been shown to accumulate P as polyphosphates when transitioning from P deplete to P replete conditions.[17] In this study we investigated the ability of microalgae to absorb lanthanides in relation to polyphosphate accumulation. Using algae to either recover lanthanides from dilute streams, or to separate different lanthanides, is often difficult, requiring knowledge of the behavior of different lanthanides with microalgae.[29] With the

https://doi.org/10.1021/acssusresmgt.4c00237
ACS Sustainable Resour. Manage. XXXX, XXX, XXX−XXX

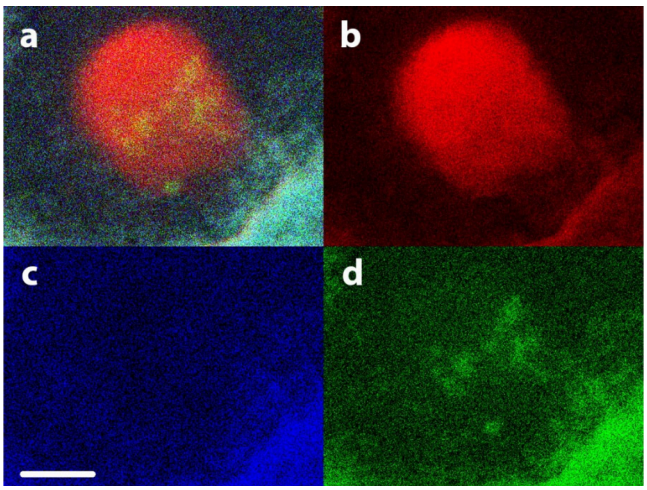

Figure 7. Coincident distribution EDS maps of three elements in *Chlamydomonas reinhardtii* with added Gd: (a) composite elemental map containing C, Gd, and P, using the colors from photos (b), (c), and (d); (b) map of C (K) in red; (c) map of Gd (L) in blue; (c) map of P (K) in green. Scale bar 2.5 μm. In the composite image, P + Gd appears as cyan and Gd + P + C appears as yellow.

model alga *C. reinhardtii* chosen here, it is apparent that this behavior is different for Ce and Gd.

Lanthanides are known to affect the growth of microalgae. This is an important consideration if this technique is to be used as for lanthanide accumulation or separation. Ce has been found to decrease photosynthetic yield in *C. reinhardtii* in concentrations from 1 μM and to 200 μM,[30] and increasing Ce^{3+} concentrations trigger oxidative stress response.[31,30] In contrast, another study found Ce^{3+} at low concentrations (up to 7 μM) to slightly boost production of *Chlorella* green microalgae.[32] In our work, the concentration of Ce^{3+} was 24 μM Ce^{3+} (and of Gd^{3+} 38 μM), so while growth inhibition could have occurred, we did not observe any significant changes in optical density over the course of the experiment (Table 1).

There are significant differences in the chemistry of Ce and Gd, which could be expected to result in differences in uptake of these elements by microalgae. The Ce^{3+} and Gd^{3+} states are normally the thermodynamically favored states in biological environments. Ce, one of the first elements in the lanthanide series, is relatively abundant in nature and has known uses in biological processes. Gd, which is about the middle of the lanthanide series, is less involved in known biological processes.[33] Size differs between the two ions, with Ce(III) having an ionic radii of 1.01 Å and Gd(III) of 0.938 Å for 6-coordinate sites.[34] This value further decreases along the lanthanide series, which alters the stability of compounds formed with these rare earth ions.

We observed that while some Gd appears to enter the cells of *C. reinhardtii*, Ce did not, so there may be a selective barrier to the entry of these ions. The potential involvement of the cell wall as a barrier to Ce entry has been investigated in this microalga, involving a wild type and a cell wall−free mutant, but this was found not to significantly control the toxicity of Ce.[30] In the red alga *Galdieria sulphuraria*, the accumulation of La, Nd, and Dy worked better with live cells than with dead cells, suggesting active transport.[35]

The storage sites for metals within algae (and in other plants or in cyanobacteria) vary depending on the metal and the organism. Some elements have been observed to concentrate in chloroplasts, such as Nd and Ce in the green alga *Desmodesmus quadricauda*,[12] Nd in the green alga *Euglena gracilis*,[13] and Au as a non-physiological metal in the land plant *Brassica juncea*.[36] Other metals are stored in the cytoplasm, for example, La and Gd in *Desmodesmus quadricauda*,[12] and Au in *Chlorella vulgaris*.[37] Metals may be stored by surface adsorption too, as for example La, Y, and Sm physically adsorbed onto the surface of the red alga *Galdieria sulphuraria*.[9]

Bacteria have been shown to use lanthanides,[33,38] and may also store these elements. In the bacterium *Methylorubrum extorquens*, the hyperaccumulation of Gd has been observed intracellularly in a body coined the "lanthasome" in analogy to the acidocalcisome.[39] In ciliates, Gd-rich particles have been observed intracellularly in bodies containing C, O, P, Na, Mg, K, and Gd.[40]

When intracellular bodies containing polyphosphate are present in the cells of algae (and in other organisms), they provide a storage site for phosphate and, potentially, other compounds such as cations. The hypothesis of this study was that P-rich intracellular bodies could also accumulate lanthanides by precipitation or co-precipitation.. The polyphosphate-containing bodies are often considered identical to acidocalcisomes[41] and have been shown to store compounds such as Ca^{2+} or Mn^{2+}.[42] It has previously been found that polyphosphate accumulation plays a role in conferring uranium tolerance in the cyanobacterium *Anabaena torulosa*,[43] and that Ce^{3+} does not inhibit *C. reinhardtii* growth when the Ce is stabilized by phosphate, probably because it precipitates from solution.[30]

In the work presented here, Ce is not co-precipitated with phosphate as distinct intracellular bodies but does form rich Ce phosphate regions outside *C. reinhardtii* cells. In contrast, Gd is co-precipitated with phosphate as intracellular bodies. The level of Gd elsewhere in the cells is much lower, although Gd appears to be abundantly adsorbed outside *C. reinhardtii* cells.

Importantly, we found that Gd and Ce react with phosphate to form a distinct compound apparent in XANES of bulk samples. However, this compound is not found in the P granules that coincide with Gd inside the alga. It could be that Gd-polyphosphates (e.g. phytate) is formed within the granule, while outside there is a simple Gd or Ce phosphate compound. Other more detailed work on similar samples with STXM and dedicated XAS bulk analysis has shown the P-containing granules to be a phosphate compound, likely a polyphosphate of a complex nature similar to phytic acid,[17] and the spectra extracted here from STXM are consistent with this. The P K-edge XAS of the P-containing granules is similar in both the Gd- and Ce-containing algae.

During this study, the microalga *C. reinhardtii* accumulated 17% of the Ce and 27% of the Gd available (i.e. 2.7 mg·L^{-1}). This is at the low end of the range of concentrations of rare earths typically found in mining waste[44] therefore the method could be suitable for such waste. However, the system presented here was not optimized for rare earth accumulation. With optimization and a longer contact time, or more than one contact between the microalga and the solution, a significant recovery of lanthanide from solution could probably be achieved. Further research is needed.

Mixtures of lanthanides, which is normally how rare earth elements are found, can be difficult to separate because of their similar physical and chemical properties.[45] The clear differences found in this study between the behavior of Ce and Gd,

https://doi.org/10.1021/acssusresmgt.4c00237
ACS Sustainable Resour. Manage. XXXX, XXX, XXX−XXX

two lanthanide series elements that accumulate in microalgae, may point to a potential biological separation process that could be used with lanthanide ores. Microalgae containing P granules could therefore potentially be used either to collect lanthanides from dilute solutions or to separate solutions of lanthanides into individual rare earth elements. Further studies are critically needed to evaluate the feasibility of using microalgae to extract specific rare earth elements from complex solutions that contain other rare earths and, in most cases, other metals.

The STXM technique enables mapping of chemistry (chemical structure, not just elemental composition) to be investigated for a combination of light and heavy elements at high spatial resolution, with appropriate choice of X-ray absorption edges for the elements of interest. The new SoftiMax beamline at MAX IV (Lund, Sweden) has been shown to be a powerful and capable instrument for such studies. This study illustrates the capabilities of the beamline to image at high spatial resolution and high energy resolution in this X-ray energy region, and is the first to use the low-energy range for the STXM beamline on SoftiMax at the MAX IV synchrotron. The images here represent only part of the spatial resolution possible, with the potential for higher spatial resolution. Changing from the 2145 eV P K-edge to the Ce 883 eV M5-edge and the Gd 1189 eV M5-edge was simple and enabled multiple images to be taken on the same sample area without problems with registration. It also showed the capability of the beamline to image lanthanides at a low-energy X-ray absorption edge so that these elements can be mapped on the same sample regions as light elements such as P, Si, S, or Cl.

CONCLUSIONS

We stimulated the microalga *Chlamydomonas reinhardtii* to synthesize intracellular polyphosphate granules and exposed the cultures to the lanthanides Ce and Gd. The distribution of Gd, Ce, and P was mapped using STXM at the Gd $M_{4,5}$-edge, the Ce $M_{4,5}$-edge, and the P K-edge, and SEM/EDS. Mapping these elements by STXM using these low-energy absorption edges was possible, enabling the simultaneous collection of the distribution and chemistry of these heavier elements with P (a light element). Gd was associated with polyphosphate granules intracellularly and with phosphate outside of the cells. In contrast, Ce was associated with phosphate only outside the cells. Gd and Ce formed a distinct compound with P, apparent in XANES of bulk samples. However, this compound was not found in the P granules that are coincident with Gd inside the alga. Overall, our results suggest the selective accumulation of Gd by *C. reinhardtii* could enable the selective recovery of this valuable element from dilute solutions. With more research, it is possible that such microalgae-based selective techniques can be generalized to a larger array of rare earth elements.

AUTHOR INFORMATION

Corresponding Author

Richard G. Haverkamp − *School of Food Technology and Natural Sciences, Massey University, Palmerston North 4410, New Zealand;* orcid.org/0000-0002-3890-7105; Email: r.haverkamp@massey.ac.nz

Authors

Maxence Plouviez − *School of Food Technology and Natural Sciences, Massey University, Palmerston North 4410, New Zealand; Cawthron Institute, Nelson 7010, New Zealand;* orcid.org/0000-0001-6824-697X

Benoit Guieysse − *School of Food Technology and Natural Sciences, Massey University, Palmerston North 4410, New Zealand;* orcid.org/0000-0002-8711-3045

Karla Wolmarans − *School of Food Technology and Natural Sciences, Massey University, Palmerston North 4410, New Zealand*

Andrea Marie E. Matinong − *School of Food Technology and Natural Sciences, Massey University, Palmerston North 4410, New Zealand*

Olivia Buwalda − *School of Food Technology and Natural Sciences, Massey University, Palmerston North 4410, New Zealand*

Karina Thånell − *MAX IV, Lund University, 224 84 Lund, Sweden*

Igor Beinik − *MAX IV, Lund University, 224 84 Lund, Sweden*

J. R. Marius Tuyishime − *MAX IV, Lund University, 224 84 Lund, Sweden*

Valerie Mitchell − *Victoria University of Wellington, Wellington 6140, New Zealand*

Peter Kappen − *Victoria University of Wellington, Wellington 6140, New Zealand*

David Flynn − *Australian Synchrotron, ANSTO, Melbourne, Victoria 3168, Australia*

Thierry Jauffrais − *Ifremer, UMR 9220 ENTROPIE, Noumea 98848, New Caledonia*

Complete contact information is available at: https://pubs.acs.org/10.1021/acssusresmgt.4c00237

Author Contributions

The manuscript was written through contributions of all authors. All authors have given approval to the final version of the manuscript.

Notes

The authors declare no competing financial interest.

ACKNOWLEDGMENTS

The authors thank Stuart Morrow, School of Chemical Sciences, The University of Auckland for the ICP-MS analysis. Beamtime on SoftiMax was provided by MAX IV, Lund, Sweden, grant number 20220911 as part of commissioning of the STXM beamline for P. Travel funding was provided by the New Zealand Synchrotron Group capability build fund. Beamtime on MEX2 was provided by the Australian Synchrotron, ANSTO, Melbourne, Australia, grant number M21174. The work was supported by the Pacific Fund, French Embassy of New Zealand, grant number 2337 and the Ministry of Business, Innovation and Employment, Wellington, New Zealand, grant number MAUX2302.

REFERENCES

(1) Hu, Z.; Yu, B.; Liu, L. C.; Wei, Y. M. Evaluating rare-earth constraints on wind power development under China's carbon-neutral target. *Sci. Total Environ.* **2024**, *912*, 168634.

(2) Zhao, S.; Wang, P.; Chen, W.; Wang, L.; Wang, Q.-C.; Chen, W.-Q. Supply and demand conflicts of critical heavy rare earth element: Lessons from gadolinium. *Resour. Conserv. Recycl.* **2023**, *199*, 107254.

(3) Fan, J. H.; Omura, A.; Roca, E. Geopolitics and rare earth metals. *Eur. J. Polit. Econ.* **2023**, *78*, 102356.

(4) Vo, P. H.; Danaee, S.; Hai, H. T. N.; Huy, L. N.; Nguyen, T. A.; Nguyen, H. T.; Kuzhiumparambil, U.; Kim, M.; Nghiem, L. D.; Ralph, P. J. Biomining for sustainable recovery of rare earth elements from mining waste: A comprehensive review. *Sci. Total Environ.* **2024**, *908*, 168210.
(5) Zapp, P.; Schreiber, A.; Marx, J.; Kuckshinrichs, W. Environmental impacts of rare earth production. *MRS Bull.* **2022**, *47* (3), 267−275.
(6) Sedykh, A. E.; Pflug, J. J.; Schäfer, T. C.; Bissert, R.; Kurth, D. G.; Müller-Buschbaum, K. Rapid spectrometer-free luminescence-based detection of Tb^{3+} and Eu^{3+} in aqueous solution for recovery and urban mining. *ACS Sustain. Chem. Eng.* **2022**, *10* (16), 5101−5109.
(7) Birungi, Z. S.; Chirwa, E. M. N. The kinetics of uptake and recovery of lanthanum using freshwater algae as biosorbents: Comparative analysis. *Bioresour. Technol.* **2014**, *160*, 43−51.
(8) Iovinella, M.; Lombardo, F.; Ciniglia, C.; Palmieri, M.; Di Cicco, M. R.; Trifuoggi, M.; Race, M.; Manfredi, C.; Lubritto, C.; Fabbricino, M.; et al. Bioremoval of yttrium(III), cerium(III), europium(III), and terbium(III) from single and quaternary aqueous solutions using the extremophile Galdieria sulphuraria (Galdieriaceae, Rhodophyta). *Plants* **2022**, *11* (10), 1376.
(9) Sun, Y.; Lu, T.; Pan, Y.; Shi, M.; Ding, D.; Ma, Z.; Liu, J.; Yuan, Y.; Fei, L.; Sun, Y. Recovering rare earth elements via immobilized red algae from ammonium-rich wastewater. *Environ. Sci. Ecotechnology* **2022**, *12*, 100204.
(10) Jacinto, J.; Henriques, B.; Duarte, A.; Vale, C.; Pereira, E. Removal and recovery of critical rare elements from contaminated waters by living *Gracilaria gracilis*. *J. Hazard. Mater.* **2018**, *344*, 531−538.
(11) Sadovsky, D.; Brenner, A.; Astrachan, B.; Asaf, B.; Gonen, R. Biosorption potential of cerium ions using *Spirulina* biomass. *J. Rare Earths* **2016**, *34* (6), 644−652.
(12) Řezanka, T.; Kaineder, K.; Mezricky, D.; Řezanka, M.; Bišová, K.; Zachleder, V.; Vítová, M. The effect of lanthanides on photosynthesis, growth, and chlorophyll profile of the green alga Desmodesmus quadricauda. *Photosynth. Res.* **2016**, *130* (1-3), 335−346.
(13) Kang, L.; Shen, Z.; Jin, C. Neodymium cations Nd^{3+} were transported to the interior of *Euglena gracilis* 277. *Chin. Sci. Bull.* **2000**, *45*, 585−592.
(14) Huo, Z.; Chen, C.; Chu, D.; Li, H.; Li, Y. Systematic synthesis of lanthanide phosphate nanocrystals. *Chem.—Eur. J.* **2007**, *13* (27), 7708−7714.
(15) Wilharm, R. K.; Huang, S.-Y.; Gugger, I. J.; Pierre, V. C. A walk across the lanthanide series: Trend in affinity for phosphate and stability of lanthanide receptors from La(III) to Lu(III). *Inorg. Chem.* **2021**, *60* (20), 15808−15817.
(16) Cliff, A.; Guieysse, B.; Brown, N.; Lockhart, P.; Dubreucq, E.; Plouviez, M. Polyphosphate synthesis is an evolutionarily ancient phosphorus storage strategy in microalgae. *Algal Res.* **2023**, *73*, 103161.
(17) Plouviez, M.; Guieysse, B.; Buwalda, O.; Wolmarans, K.; Thånell, K.; Beinik, I.; Tuyishime, J. R. M.; Mitchell, V.; Kappen, P.; Haverkamp, R. G. Phosphorus storage in microalgae: STXM and XAS P K-edge investigation. *ACS Sustain. Res. Manag.* **2024**, *1* (6), 1270−1278.
(18) Schwenke, J.; Thanell, K.; Beinik, I.; Roslund, L.; Tyliszczak, T. Soft/MAX-A new soft X-ray microscopy and coherent imaging beamline at the MAX IV facility. *Microsc. Microanal.* **2018**, *24* (S2), 234−235.
(19) Marcus, M. A. Data analysis in spectroscopic STXM. *J. Electron Spectrosc. Relat. Phenom.* **2023**, *264*, 147310.
(20) Plouviez, M.; Fernandez, E.; Grossman, A. R.; Sanz-Luque, E.; Sells, M.; Wheeler, D.; Guieysse, B. Responses of *Chlamydomonas reinhardtii* during the transition from P-deficient to P-sufficient growth (the P-overplus response): The roles of the vacuolar transport chaperones and polyphosphate synthesis. *J. Phycol.* **2021**, *57* (3), 988−1003.
(21) Blake, A. V.; Wei, H.; Donahue, C. M.; Lee, K.; Keith, J. M.; Daly, S. R. Solid energy calibration standards for P K-edge XANES: electronic structure analysis of PPh4Br. *J. Synchrotron Rad.* **2018**, *25* (2), 529−536.
(22) Hitchcock, A. P. Analysis of X-ray images and spectra (aXis2000): A toolkit for the analysis of X-ray spectromicroscopy data. *J. Electron Spectrosc. Relat. Phenom.* **2023**, *266*, 147360.
(23) Ravel, B.; Newville, M. ATHENA, ARTEMIS, HEPHAESTUS: data analysis for X-ray absorption spectroscopy using IFEFFIT. *J. Synchrotron Rad.* **2005**, *12* (4), 537−541.
(24) Löble, M. W.; Keith, J. M.; Altman, A. B.; Stieber, S. C. E.; Batista, E. R.; Boland, K. S.; Conradson, S. D.; Clark, D. L.; Lezama Pacheco, J.; Kozimor, S. A.; et al. Covalency in lanthanides. An X-ray absorption spectroscopy and density functional theory study of $LnCl_6^{x-}(x=3, 2)$. *J. Am. Chem. Soc.* **2015**, *137* (7), 2506−2523.
(25) Dallera, C.; Braicovich, L.; Ghiringhelli, G.; Van Veenendaal, M.; Goedkoop, J.; Brookes, N. Resonant soft-x-ray inelastic scattering from Gd in the $Gd_3Ga_5O_{12}$ garnet with excitation across the M_5 edge. *Phys. Rev. B* **1997**, *56* (3), 1279.
(26) Tyszka, B.; Szade, J.; Burian, W.; Skorek, G.; Deniszczyk, J.; Sikora, M.; Zając, D.; Kapusta, C.; Matteucci, M.; Bondino, F.; et al. Investigation of Gd compounds using synchrotron radiation. *J. Alloys Compd.* **2005**, *401* (1-2), 165−172.
(27) Soni, S.; Dave, M.; Dalela, B.; Alvi, P.; Kumar, S.; Sharma, S.; Phase, D.; Gupta, M.; Dalela, S. Effect of defects and oxygen vacancies on the RTFM properties of pure and Gd-doped CeO_2 nanomaterials through soft XAS. *Appl. Phys. A* **2020**, *126*, 1−11.
(28) Shuh, D. K.; Terminello, L. J.; Boatner, L.; Abraham, M. X-ray absorption spectroscopy of the rare earth orthophosphates. *Mater. Res. Soc. Symp. Proc.* **1993**, *307*, 95.
(29) Manfredi, C.; Amoruso, A.; Ciniglia, C.; Iovinella, M.; Palmieri, M.; Lubritto, C.; El Hassanin, A.; Davis, S. J.; Trifuoggi, M. Selective biosorption of lanthanides onto *Galdieria sulphuraria*. *Chemosphere* **2023**, *317*, 137818.
(30) Röhder, L. A.; Brandt, T.; Sigg, L.; Behra, R. Influence of agglomeration of cerium oxide nanoparticles and speciation of cerium(III) on short term effects to the green algae Chlamydomonas reinhardtii. *Aquat. Toxicol.* **2014**, *152*, 121−130.
(31) Morel, E.; Dozois, J.; Slaveykova, V. I.; Wilkinson, K. J. Distinguishing the effects of Ce nanoparticles from their dissolution products: identification of transcriptomic biomarkers that are specific for ionic Ce in *Chlamydomonas reinhardtii*. *Metallomics* **2021**, *13* (1), mfaa005.
(32) Zuo, W.; Chen, Z.; Zhang, J.; Zhan, W.; Yang, H.; Li, L.; Zhu, W.; Mao, Y. The microalgae-based wastewater treatment system coupled with cerium: A potential way for energy saving and microalgae boost. *Environ. Sci. Pollut. Res.* **2023**, *30* (21), 60920−60931.
(33) Cotruvo Jr, J. A. The chemistry of lanthanides in biology: recent discoveries, emerging principles, and technological applications. *ACS Cent. Sci.* **2019**, *5* (9), 1496−1506.
(34) Lundberg, D.; Persson, I.; Eriksson, L.; D'Angelo, P.; De Panfilis, S. Structural study of the N, N′-dimethylpropyleneurea solvated lanthanoid (III) ions in solution and solid state with an analysis of the ionic radii of lanthanoid (III) ions. *Inorg. Chem.* **2010**, *49* (10), 4420−4432.
(35) Minoda, A.; Sawada, H.; Suzuki, S.; Miyashita, S.-i.; Inagaki, K.; Yamamoto, T.; Tsuzuki, M. Recovery of rare earth elements from the sulfothermophilic red alga *Galdieria sulphuraria* using aqueous acid. *Appl. Environ. Microbiol.* **2015**, *99* (3), 1513−1519.
(36) Beattie, I. R.; Haverkamp, R. G. Silver and gold nanoparticles in plants: sites for the reduction to metal. *Metallomics* **2011**, *3* (6), 628−632.
(37) Luangpipat, T.; Beattie, I. R.; Chisti, Y.; Haverkamp, R. G. Gold nanoparticles produced in a microalga. *J. Nanopart. Res.* **2011**, *13* (12), 6439−6445.
(38) Peplow, M. Unlocking the Lanthanome. *ACS Cent. Sci.* **2021**, *7* (11), 1776−1779.

https://doi.org/10.1021/acssusresmgt.4c00237
ACS Sustainable Resour. Manage. XXXX, XXX, XXX−XXX

(39) Good, N. M.; Lee, H. D.; Hawker, E. R.; Su, M. Z.; Gilad, A. A.; Martinez-Gomez, N. C. Hyperaccumulation of gadolinium by *Methylorubrum extorquens* AM1 reveals impacts of lanthanides on cellular processes beyond methylotrophy. *Front. Microbiol.* **2022**, *13*, 820327.
(40) Kohl, J.; Schweikert, M.; Klaas, N.; Lemloh, M.-L. Intracellular bioaccumulation of the rare earth element gadolinium in ciliate cells resulting in biogenic particle formation and excretion. *Sci. Rep.* **2023**, *13* (1), 5650.
(41) Frank, C.; Jendrossek, D. Acidocalcisomes and polyphosphate granules are different subcellular structures in *Agrobacterium tumefaciens*. *Appl. Environ. Microbiol.* **2020**, *86* (8), e02759−02719.
(42) Diaz, J.; Ingall, E.; Vogt, S.; de Jonge, M. D.; Paterson, D.; Rau, C.; Brandes, J. A. Characterization of phosphorus, calcium, iron, and other elements in organisms at sub-micron resolution using X-ray fluorescence spectromicroscopy. *Limnol. Oceanogr. Methods* **2009**, *7*, 42−51.
(43) Chandwadkar, P.; Acharya, C. Inorganic polyphosphate accumulation protects a marine, filamentous cyanobacterium, *Anabaena torulosa* against uranium toxicity. *J. Environ. Radioact.* **2023**, *263*, 107185.
(44) Mwewa, B.; Tadie, M.; Ndlovu, S.; Simate, G. S.; Matinde, E. Recovery of rare earth elements from acid mine drainage: A review of the extraction methods. *J. Environ. Chem. Eng.* **2022**, *10* (3), 107704.
(45) Baldwin, A. G.; Ivanov, A. S.; Williams, N. J.; Ellis, R. J.; Moyer, B. A.; Bryantsev, V. S.; Shafer, J. C. Outer-sphere water clusters tune the lanthanide selectivity of diglycolamides. *ACS Cent. Sci.* **2018**, *4* (6), 739−747.

https://doi.org/10.1021/acssusresmgt.4c00237
ACS Sustainable Resour. Manage. XXXX, XXX, XXX−XXX